BIOCHEMISTRY
including biophysical chemistry & molecular biology

Article

pubs.acs.org/biochemistry

A Model for the Flexibility of the Distal Histidine in Dehaloperoxidase-Hemoglobin A Based on X-ray Crystal Structures of the Carbon Monoxide Adduct

Junjie Zhao, Vesna de Serrano, and Stefan Franzen*

Department of Chemistry, North Carolina State University, Raleigh, North Carolina 27695, United States

Supporting Information

ABSTRACT: Dehaloperoxidase hemoglobin A (DHP A) is a multifunctional hemoglobin that appears to have evolved oxidative pathways for the degradation of xenobiotics as a protective function that complements the oxygen transport function. DHP A possesses at least two internal binding sites, one for substrates and one for inhibitors, which include various halogenated phenols and indoles. Herein, we report the X-ray crystallographic structure of the carbonmonoxy complex (DHPCO). Unlike other DHP structures with 6-coordinated heme, the conformation of the distal histidine (H55) in DHPCO is primarily external or solvent exposed, despite the fact that the heme Fe is 6-coordinated. As observed generally in globins, DHP exhibits two distal histidine conformations (one internal and one external). In previous structural studies, we have shown that the distribution of H55 conformations is weighted strongly toward the external position when the DHP heme Fe is 5-coordinated. The large population of the external conformation of the distal histidine observed in DHPCO crystals at pH 6.0 indicates that some structural factor in DHP must account for the difference from other globins, which exhibit a significant external conformation only when pH < 4.5. While the original hypothesis suggested that interaction with a heme-Fe-bound ligand was the determinant of H55 conformation, the current study forces a refinement of that hypothesis. The external or open conformation of H55 is observed to have interactions with two propionate groups in heme, at distances of 3.82 and 2.73 Å, respectively. A relatively weak hydrogen bonding interaction between H55 and CO, combined with strong interactions with heme propionate (position 6), is hypothesized to strengthen the external conformation of H55. Density function theory (DFT) calculations were conducted to test whether there is a weaker hydrogen bond interaction between H55 and heme bonded CO or O_2. Molecular dynamics simulations were conducted to examine how the tautomeric forms of H55 affect the dynamic motions of the distal histidine that govern the switching between open and closed conformations. The calculations support the modified hypothesis suggesting a competition between the strength of interactions with heme ligand and the heme propionates as the factors that determine the conformation of the distal histidine.

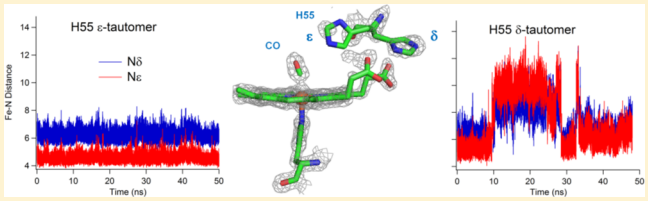

Dehaloperoxidase isoenzyme A (DHP A),[1,2] first isolated from the terebellid polychaete *Amphitrite ornata*, is a hemoprotein that appears to function as both a hemoglobin and a peroxidase. There are two isoforms known as DHP A and B.[3,4] Statements true of both isoforms may simply refer to DHP to mean both DHP A and B. As a hemoglobin, the heme Fe of DHP A can cycle between the deoxy and oxy state by reversibly binding with O_2, which is used for oxygen storage and transport. As a peroxidase, DHP A can catalyze the oxidization of 2,4,6-trihalophenol (2,4,6-TXP) to the corresponding 2,6-dihaloquinone (2,6-DXQ) (X = I, Br, Cl, F) using H_2O_2 as a cosubstrate.[2,5] Globin function requires a ferrous heme Fe (Fe^{2+}) to reversibly bind with O_2. However, peroxidase function favors a ferric heme Fe (Fe^{3+}) for catalytic oxidation of the substrate 2,4,6-TXP in the presence of H_2O_2. The mutual exclusivity of Fe^{2+} and Fe^{3+} in these two functions leads to a paradox in DHP function.[6] Recent studies have shown that DHP can be activated by H_2O_2 for peroxidase function starting from the oxyferrous state, which makes DHP a unique peroxidase-hemoglobin dual functional enzyme.[7,8] The observation of an internal substrate binding site by X-ray crystallography[9,10] has also helped to resolve the paradox since it suggests that substrate binding may function as a trigger for the switch from globin to peroxidase function by its strong interaction with the heme Fe. One can identify both an electrostatic component[11,12] in addition to a steric effect due to substrate binding.[13,14] The observation of a time-resolved X-ray crystal structure is consistent with the open distal pocket in DHP.[15] The distal histidine, H55, is clearly involved in the entrance and exit of the substrate.[16] We have hypothesized that the unusual flexibility of H55 is linked to its role in the triggering the functional switch in DHP,[17,18] by analogy to the flavohemoglobins.[19] The role of the flexible histidine in functional switching has an analogy in heme oxygenase-1, which can switch to a peroxidase function if the distal histidine hydrogen bonding to heme-bound H_2O is disrupted.[20] Another

Received: February 12, 2014
Revised: March 26, 2014
Published: March 27, 2014

   dx.doi.org/10.1021/bi5001905 | *Biochemistry* 2014, 53, 2474−2482

means for introducing functional diversity involves the conformations of distal glutamate and axial ligation by cysteine, as observed in chloroperoxidase.[21] Flexibility can also lead to inactivation by formation of a bis-histidine adduct with both proximal and distal histidines bound to the heme Fe. This type of behavior is observed in the W41A mutant of soybean ascorbate peroxidase.[22] Thus, flexibility is a double-edged sword, and the competition between enhanced catalytic activity and inactivation due to six-coordinate heme formation is observed in the M86A mutant of DHP.[23] The energetic basis for flexibility of the distal ligand needs to be understood in more detail if we are to understand multifunctional proteins.

There are no polar amino acids in the distal pocket of native DHP aside from H55. In this regard, DHP is different from peroxidases, which typically have at least one polar amino acid to participate in activation of bound H_2O_2.[24−26] As consequence, H55 is the only possible amino acid that can play a role in the heterolytic bond cleavage of Fe-bound H_2O_2 during peroxidase function. Therefore, the communication of the distal pocket with H55 is still a central issue in structural and functional studies of DHP. In previous studies, two conformations of distal histidine H55 have been observed identified as external ("open") and internal ("closed") conformation by analogy with similar observations in sperm whale myoglobin (SWMb).[27,28] The role played by the histidine in DHP is similar to that observed in human Hb as observed by NMR spectroscopy.[29] Yet, the conformation of H55 in DHP is strongly affected by the binding of phenolic substrates and inhibitors,[30,31] which is a unique feature of DHP. The closed conformation is observed when H55 points inside the distal pocket and interacts with the sixth ligand (i.e., H_2O, O_2) of heme Fe (PDB 2QFK, 2QFN).[18,32] This conformation is similar, but not identical, to Mb[33,34] and Hb[35,36] structures. The functional relevance of the histidine in regulating small ligand binding has been a central feature of studies of both Hbs[37] and Mbs.[38] The bound states can be compared using the π-backbonding correlation for CO,[39] suggesting that the weaker hydrogen bonding of the distal histidine with the CO of DHP[40] has similarity with trout Mb.[41] The open conformation refers to H55 rotated to a solvent-exposed position. This is observed corresponding to a 5-coordinated heme Fe either in deoxyferrous DHP structure (PDB 3DR9) or when inhibitors 4-XP (X = F, Cl, Br, and I) (PDB 3LB1, 3LB2, 3LB3, 3LB4) are present in distal pocket.[17,18,42] This dynamic motion of the distal histidine has been associated with entrance and exit of small ligands to and from the distal pocket by a hypothesis that dates back nearly 50 years[35] and has been extensively studied in the interim by experimental[43,44] and computational methods[45,46] When residue T56, immediately adjacent to H55, is mutated to a series of hydrophobic amino acids, it is evident that this position has a large steric effect on the flexibility of H55.[47,48] On the basis of these structures and spectroscopic data, we have hypothesized that there is a correlation between the Fe ligation state and the conformation of H55. In 6-coordinated heme adducts of DHP A, H55 is in the closed conformation where it can stabilize the sixth ligand by hydrogen bonding. In 5-coordinated heme adducts of DHP, H55 is in open (solvent exposed) conformation because there is no sixth ligand available for hydrogen bonding interaction. To test the validity of the hypothesis for the carbon monoxide form of DHP A (DHPCO), we have determined the X-ray crystal structure of three different DHPCO crystals prepared using different methods.

The context for these studies is evident from the extensive studies of the CO form of SWMb. For the past 50 years, studies of carbonmonoxy sperm whale myoglobin (SWMbCO) have attempted to explain the discrimination against CO in normal globin function.[43,49−51] Free heme has an affinity for CO that is ~20 000 times greater than that for O_2, while the heme in SWMb has a ratio of affinities of only ~25.[51,52] The two major factors that have been hypothesized to account for the difference in the protein are steric interactions and hydrogen bonding.[43,52,53] For 40 years, it was thought that CO bound to the heme iron in an unfavorable bent conformation. Since O_2 binds in a bent conformation, the bent form of CO would have lower binding affinity relative to O_2, potentially be one way to discriminate against CO binding. In the mid-1990s, infrared dichroism of single crystals revealed that the Fe−C−O bend angle is essentially 180°, but rather the Fe−C−O triad had a small tilt of ~7° from the normal to the heme plane.[49,50] The structures showing this nearly upright structure for the CO molecule were a surprise when they first were published, because they contradicted an idea that had been in the literature for nearly 40 years.[54,55] The structures led to an alternative hypothesis that the difference in hydrogen bond strength is the major factor that leads to a stabilization of O_2 relative to CO.[34,56] In SWMb, the interactions of the distal histidine are not usually viewed as a competition between the open (external) and closed (internal) conformers, since the H64 is predominantly in the internal site under any but extreme conditions of pH.[27] However, the nature of the interaction may be different in DHP because of the greater flexibility of H55 relative to H64 in SWMb. Therefore, the interaction of H55 with CO molecule will be a key aspect of the X-ray crystallographic structures of DHPCO. In addition, density functional theory (DFT) calculations conducted to test the interactions between H55 and heme-bonded CO or O_2 provide us with a quantitative comparison in the energies of different tautomers of H55 in CO and O_2 adducts.[56−63] Finally, molecular dynamics (MD) simulations provide a link between the computational results and X-ray crystal structures by showing the dynamic consequences of different tautomeric forms of the distal histidine H55.[34,46,64]

MATERIALS AND METHODS

Purification and Crystallization of DHP. The non-6X-His tagged form of the DHP A protein was expressed, purified, and prepared in the ferric form as previously described.[18,32] DHPCO complex crystals were obtained from two different methods. In the first method, ferric DHP crystals were grown by the hanging-drop vapor-diffusion method from 0.2 M ammonium sulfate and 34% poly(ethylene glycol) 4000 at 277 K. Crystals were reduced with two different reducing agents, sodium dithionite (NaS_2O_6) or dithiothreitol (DTT), and incubated in a CO atmosphere for 3 h. The corresponding PDB codes of two crystals obtained from the above method are 4DWT (DHPCO-2, reduced by NaS_2O_6) and 4DWU (DHPCO-3, reduced by DTT), respectively. In the other method, a ferric DHP solution was reduced by 20-fold excess sodium dithionite first, and crystals were grown by the hanging-drop vapor-diffusion method from 0.2 M ammonium sulfate and 29% poly(ethylene glycol) 8000 at 277 K in 1 atm CO atmosphere. The corresponding crystal obtained was assigned to PDB 4GZG (DHPCO-1). The starting protein concentration was 8 mg mL^{-1} in 10 mM Na cacodylate pH 6.5 buffer for both methods.

dx.doi.org/10.1021/bi5001905 | Biochemistry 2014, 53, 2474−2482

X-ray Data Collection and Structure Refinement. The DHPCO-1 data set was collected on the 14-BM-C beamline of the APS synchrotron facility, whereas the DHPCO-3 data set was collected on the 22-BM beamline. DHPCO-2 data set was collected on the in-house Rigaku Cu rotating anode X-ray generator RUH3R at NCSU X-ray core facility. All the data sets were processed using the HKL2000 program suite.[65] The structure determination and refinement calculations were performed using the CCP4 suite of programs.[66,67] Visualization and manual model building were conducted using the Coot model building software.[68] The carbon monoxide molecule was placed in the center of the electron density on top of heme iron as a separated chain, with no other restraints. Several refinements were conducted to get the best CO geometry and position in both $F_o - F_c$ and $2F_o - F_c$ maps. The final DHPCO-1 (4GZG), DHPCO-2 (4DWT), and DHPCO-3 (4DWU) structures were refined to R/R_{free} values of 17.7/20.9%, 20.8/24.5%, and 17.9/20.2%, respectively. The DHPCO-1 model contains two polypeptide chains, three sulfate ions, and 244 water molecules. The DHPCO-2 model contains two polypeptide chains, five sulfate ions, and 147 water molecules. The DHPCO-3 model contains two polypeptide chains, five sulfate ions, and 191 water molecules. The data-collection and model refinement statistics for the X-ray data sets are summarized in Table 1.

DFT Calculations. DFT calculations were carried out using the DMol3 program.[69,70] Geometry optimization was carried out using the PBE functional[71] and the numerical DNP basis set. Structures were geometry optimized until the convergence criterion of 10^{-6} Hartrees was reached for the energy difference between successive minimization steps. For these relatively large calculations (208 atoms), the THERMAL option was used to ensure convergence.[72] This option is based on a grand canonical ensemble approach to electron occupation. The final energy is obtained by extrapolation to $T = 0$ K. Calculations were carried out at the high performance cluster (HPC) at North Carolina State University and using the ARC computing resource.

The models for DFT used in this study were composed of truncations of two X-ray crystal structures (PDB 2QFN for DHP-O_2 and PDB 4GZG for DHPCO). In model 1, the amino acids used are residues F24, Y34, H55, T56, E57, K58, V59, and H89. The residues F24 and Y34 are the two aromatic amino acids nearest to the bound diatomic ligand. Residues 55−59 form an arc surrounding the bound diatomic ligand and comprise the nearest amino acids on the opposite side to F24 and Y34. H89 is the proximal histidine, which ligates to the heme Fe atom. The single amino acids were truncated at the α-carbon, meaning that the α-carbon is represented by a methyl group, and the amide N and carbonyl C are converted to hydrogen atoms. The nomenclature for these models is 2QFN1 and 4GZG1 for the DHP-O_2 and DHPCO structures, respectively. The second model is identical to the first except that residue 38 was added in both structures. Y38 is relatively far from the heme Fe atom (i.e., Fe···O distance is ∼6.2 Å). However, on the basis of previous crystal structures, Y38 has a potentially strong interaction with H55 leading to a possible specific role for this amino acid. By performing two calculations, we have separated this effect. The nomenclature for the models that include Y38 is 2QFN2 and 4GZG2 for the DHP-O_2 and DHPCO structures, respectively. In addition, a calculation was conducted in which the O_2 in the 2QFN structure was replaced by CO. This was a control calculation to ensure that the starting point of the calculation (obtained from the X-ray crystal structure) did not bias the result in terms of either energy or structure.

Table 1. Data Collection and Refinement Statistics[a]

	DHPCO-1[e]	DHPCO-2[e]	DHPCO-3[e]
PDB code	4GZG	4DWT	4DWU
space group	$P2_12_12_1$	$P2_12_12_1$	$P2_12_12_1$
unit cell parameters			
a (Å)	57.73	57.91	57.92
b (Å)	67.27	67.47	67.62
c (Å)	69.06	68.72	68.39
Data collection			
temperature (K)	100	100	100
wavelength (Å)	0.979	1.54	0.913 39
resolution (Å)	50−1.49 (1.52−1.49)	48.2−2.10 (2.43−2.10)	44.2−1.44 (1.48−1.44)
unique reflections	44696 (2040)	16541 (898)	43419 (1931)
completeness (%)	99.5 (91.7)	99.7 (95.0)	93.9 (89.50)
R_{merge}[b] (%)	5.5 (39.6)	13.1 (49.0)	4.7 (39.7)
$I/\sigma(I)$	38.0 (4.6)	7.9 (2.32)	24.6 (3.2)
redundancy	7.0 (6.5)	4.8 (5.0)	4.3(3.7)
Refinement			
R_{work}[c] (%)	17.7	18.0	17.9
R_{free}[d] (%)	20.9	23.2	20.2
no. of atoms			
protein	2632	2607	3057
water	244	147	191
r.m.s. deviation from ideal			
bond length (Å)	0.026	0.013	0.011
bond angle (deg)	2.268	1.54	2.737

[a]Values in parentheses are for the highest resolution shell. [b]$R_{merge} = \sum_{hkl}\sum_i|I_i(hkl) - \langle I(hkl)\rangle|/\sum_{hkl}\sum_i I_i(hkl)$, where $I_i(hkl)$ is the ith measurement and $\langle I(hkl)\rangle$ is the weighted mean of all measurements of $I(hkl)$. [c]$R_{work} = \sum|F_o - F_c|/\sum|F_o|$, where F_o and F_c are the observed and calculated structure factors, respectively. [d]R_{free} is the R factor for the subset (5%) of reflections selected before and not included in the refinement. [e]DHPCO-1 was crystallized from deoxyferrous DHPA solution in CO atmosphere. DHPCO-2 was prepared by reducing ferric DHPA crystals in sodium dithionite followed by incubation in CO for 3 h; DHPCO-3 was prepared by reducing ferric DHPA crystals in DTT followed by incubation in CO for 3 h.

The α-carbons were fixed in the DFT calculation, but all other atoms were free to geometry optimize. Since the collected atoms are normally constrained by the protein, it was reasoned that fixing the α-carbons would serve as an analogous constraint for the positions of the amino acids relative to the heme Fe. The coordinates for the smaller model and the numbers of the fixed atoms are given in the Supporting Information. The geometry optimization was carried out based on Cartesian coordinates. Use of redundant coordinates, which is recommended for many calculations, fails for the large system used here since they oscillate near the minimum and do not converge. The final structures were visualized in VMD by conversion of output files to PDB format. These outputs and the input files and fixed atoms are provided in the Supporting Information.

MD Simulations. To determine whether there is any tendency for the distal histidine to fluctuate to the open position when CO is bound to the heme Fe, models were constructed of DHP A based on the PDB 4GZG X-ray crystal

dx.doi.org/10.1021/bi5001905 | Biochemistry 2014, 53, 2474−2482

structure. These models solvated and placed in a unit cell of dimensions 57.8 Å × 64.1 Å × 48.8 Å with 9254 water molecules. DHP has one negative charge which was compensated by a sodium atom. The visualization and setup of the MD simulation were carried out using the graphical user interface VMD.[73] The DHP monomer models were geometry optimized using NAMD with the CHARMM27 force field.[74,75] The parameters for the heme were modified to include the CO bonded to the heme Fe. The charges for the CO and Fe in this model were modified based on a DFT calculation using the electrostatic potential fitting (ESP) option in DMol3. (Accelrys, Inc.). A molecular dynamics simulation was run for 50 ns using NAMD with the following parameters: time step of 2 fs (SHAKE algorithm implemented), temperature of 298 K with Langevin damping, cutoff distance of 12 Å with a 1.0 Å switching distance. The simulation was run for two modifications of the structure, one with the δ-tautomer and one with the ε-tautomer of the distal histidine (H55). It was essential to carry out two parallel simulations since the tautomeric state of H55 is fixed for a given structure. The amino acids are designated HSD and HSE for the δ- and ε-tautomer, respectively.

RESULTS

X-ray Crystallographic Structures of DHPCO. Figure 1 shows the electron density of H55 in both chain A and B in DHPCO-1 (PDB 4GZG). H55 is primarily in the external position when CO is bound to heme Fe. The occupancy of CO is 1.0 and the occupancies of external and internal H55 are 90% and 10%, respectively, in both chains. The percentages are based on occupancies of CO found from the $F_o - F_c$ omit map. Although the density for the internal conformation appears to be incomplete (based on the $2F_o - F_c$ view at a cutoff of 1.5σ) shown in Figure 1, the density does not fit well to an internal H_2O molecule and indeed has the appearance of a histidine when a cutoff of 0.5σ is used (see Figure S3, Supporting Information). On the basis of the average distances in the structures, the distance from the H55 Ne to the O atom of bound CO is >10.0 Å and ~3.65 ± 0.16 Å for the external (90%) and internal (10%) conformations, respectively. DHPCO-2 (PDB 4DWT) and DHPCO-3 (PDB 4DWU) are highly similar to DHPCO-1 (see Supporting Information, Figures S1 and S2). The occupancies of distal histidine and CO and geometries of bound CO of these three different DHPCO crystals are summarized in Table 2. The similarity in the observed structures suggests that the DHPCO structure is independent of preparation methods and the reducing agent used in the experiment. The CO appears to have a slightly bent geometry when bound to the heme Fe with C−O angles ranging from 31° to 11° from the heme normal (Table 2). The structures in this study are at lower resolution compared to the most recent high resolution structures in SWMb where the angle of the Fe−C−O was determined to be a tilt that was 7°.[33] We attribute the larger Fe−C−O angle to the lower resolution of these structures relative to the very high resolution SWMbCO structures.[27,76] Figure 2 shows the overall structure of DHPCO-1 (Figure 2A) and a detailed structure of heme and distal histidine H55 (Figure 2B). Only the dominant (external) conformation of H55 is shown in both 2A and 2B. Figure 2B shows that the distances between the N^{ε} of external H55 and the two propionate groups of the heme are 3.82 ± 0.03 Å (propionate 7) and 2.73 ± 0.03 Å (propionate 6) in subunit A. The distances in the B subunit are 3.76 ± 0.08 Å (propionate 7) and 3.21 ± 0.03 Å (propionate 6). These observations indicate that a hydrogen bonding interaction between N^{ε} of

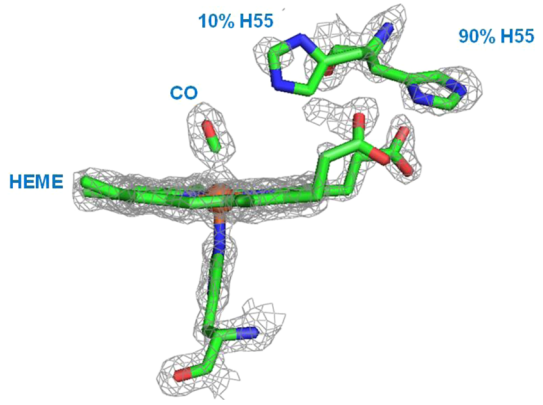

Figure 1. The $2F_o - F_c$ electron density map of the distal pocket in Chain A in DHPCO-1 (PDB 4GZG) is shown. The occupancy of external H55 and internal H55 is 90% and 10% respectively in both Chains A and B, although only Chain A is shown. The cutoff used in this figure is 1.5σ.

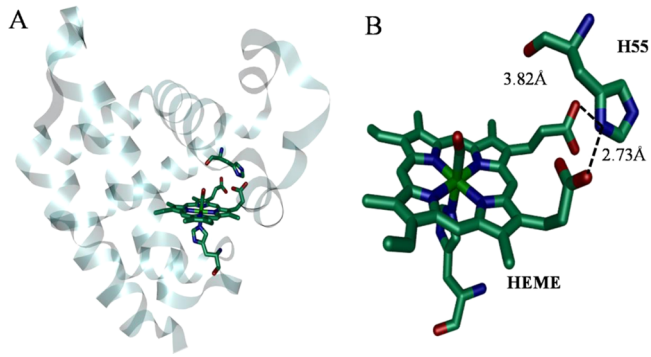

Figure 2. The overall structure of DHPCO-1 (Chain B) is shown on left (A); the interaction between two heme propionate groups and external H55 is shown on right, and the distances between N^{δ} and two propionates (positions 6 and 7) are 2.73 and 3.82 Å (B). Only the majority conformation of H55 (external) is shown.

Table 2. Occupancies and Geometries of Three Different DHPCO Crystals, Either Obtained from Different Methods or Reduced by Different Reducing Agents

crystals	Fe−CO distance (Å)		Fe−C−O angle (deg)		CO occupancy		H55 external occupancy		H55 internal occupancy	
chains	A	B	A	B	A	B	A	B	A	B
DHPCO-1	2.2	2.05	163.3	160.8	1.0	1.0	0.9	0.9	0.1	0.1
DHPCO-2	2.18	1.90	168.5	149.2	1.0	0.8	0.76	0.75	0.24	0.25
DHPCO-3	1.88	1.86	161.1	159.4	1.0	0.8	0.76	0.75	0.24	0.25

dx.doi.org/10.1021/bi5001905 | Biochemistry 2014, 53, 2474−2482

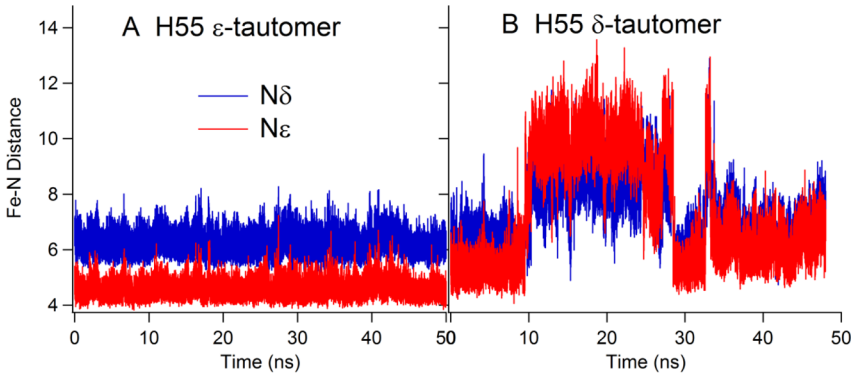

Figure 3. The distance from the Fe atom to the δ- and ε-N atoms of H55 is shown as a function of the simulation time for a MD simulation. (A) The simulation was conducted for the ε-tautomer of H55. (B) The simulation was conducted for the δ-tautomer of H55.

H55 and the heme propionate (position 6) is an important factor stabilizing the external conformation of H55.

DFT Calculations and MD Simulations. The geometry optimized structures obtained from DFT calculations conducted on a model containing 208 atoms based on the X-ray crystal structures for DHPCO (PDB 4GZG) and DHP-O_2 (PDB 2QFN) are shown in Figure S5, Supporting Information. The energies of the corresponding structures are given in Table 4. The energy for the ε-tautomer relative to the δ-tautomer is lower for the O_2 structures than for the CO structures. This corresponds to a stronger hydrogen bond formed between the histidine N−H and the bound diatomic O_2 molecule than for the CO molecule. The competing interaction for the histidine (still in the internal position in these structures) results from the hydrogen bonding interaction with heme propionate groups. We have selected only the internal (closed) conformation of H55 in the PDB 4GZG structure for modeling using DFT geometry optimization. The fact that H55 migrates slightly toward the propionate side chain in the ε-tautomer is a consequence of the hydrogen bonding interaction calculated using DFT.

The results of two 50 ns simulations for the ε- and δ-tautomers of DHP A are shown in Figure 3, panels A and B, respectively, in terms of the distances between the N atoms of H55 and the heme Fe atom. The Fe−N^{δ} and Fe−N^{ε} distances are essentially constant for the ε-tautomer shown in Figure 3A, in which H55 remains in the closed conformation throughout the simulation. H55 is locked in place by a weak, but attractive interaction between the N−$H^{\delta/\varepsilon}$ of H55 and bound CO. The distance of 4.58 ± 0.20 Å and 6.25 ± 0.26 Å for the N^{ε} and N^{δ} atoms with respect to the Fe atom indicates that H55 is in proximity to the CO in a manner that is evident from the DFT calculations discussed above (see Figure S5, Supporting Information). On the other hand, the simulation for the δ-tautomer of H55 shows a much greater flexibility of H55, which is consistent with two conformations (Figure 3B). The same conclusion is reached if the C_{α}−C_{β}−C_{γ}−N_{δ} dihedral angle is plotted (see Figure S4, Supporting Information). These positions of H55 in these conformations correspond well to the two conformations of H55 observed in several X-ray crystal structures.[16,18,32,42,77] The MD simulation suggests an approximately equal population of each conformer.

DISCUSSION

Structural Evidence for Flexibility of the Distal Histidine in DHP A. The flexibility of the distal histidine, H55, in DHP has been the subject of numerous studies.[12,14,17,18,42] On the basis of different X-ray crystal structures obtained at 100 K, we have hypothesized that there is a correlation between the ligation state of heme Fe and the conformation of H55. For example, H55 is observed in the internal conformation in metaquo (2QFK), metacyano (3KUN), and oxyferrous (2QFN) structures when heme Fe coordinates with H_2O, CN^-, and O_2 as the sixth ligand, respectively.[32,77] H55 possesses an external conformation in the deoxyferrous (3DR9) structure, in which heme Fe is 5-coordinate.[18] Additionally, H55 is observed in the external position when inhibitors such as 4-XPs (X = I, Br, Cl, and F) are present in ferric DHP A (3LB1, 3LB2, 3LB3, 3LB4). In these structures, the various 4-XPs are located in the distal pocket of DHP, expel the water molecule, and result in a 5-coordinated heme Fe.[42] The correlation between 6-coordinate ligation state of the heme Fe and the internal conformation of H55 has been corroborated by resonance Raman and EPR spectroscopies.[42,78,79]

The observation of an external conformation for H55 in the DHPCO structure is surprising in the context of the structural correlation observed in a series of X-ray crystal structures (e.g., 2QFK, 2QFN, 3KUN, 3DR9, 3LB1, 3LB2, 3LB3, and 3LB4).[16,18,32,42,77] The DHPCO structure provides the first example in which the distal histidine H55 is primarily in the external position in a 6-coordinated DHP structure. The observation of CO in an external conformation under the conditions used here (pH 6) is also unique among globins generally, since all other globin structures (with one exception)[27] show the distal histidine in an internal conformation. The only X-ray crystal structure in SWMbCO which shows the external H55 conformation was obtained at pH 4.[27]

Role of Hydrogen Bonding in Stabilizing the Distal Histidine Conformation. In 6-coordinate DHP structures obtained previously (metaquo, metacyano, and oxyferrous DHP), the internal conformation of H55 is stabilized by hydrogen bonding to the sixth ligand (H_2O, CN^-, and O_2, respectively) of the heme Fe.[32,77] The neutron diffraction structure of oxyferrous $SWMbO_2$ shows a hydrogen bond between distal histidine and heme bound O_2 based on the deuterium signal.[53] However, there is no deuterium signal in the corresponding position in the SWMbCO neutron diffraction structure, which suggests that there is no hydrogen bond formed between heme bound CO and the distal histidine.[80] Calculations support the observed difference, since the hydrogen bond energy of the distal histidine with

dx.doi.org/10.1021/bi5001905 | Biochemistry 2014, 53, 2474−2482

either CO or O_2 was calculated to be 8 or 32 kJ/mol, respectively.[81] We propose that the weakness of hydrogen bonding between heme bound CO and H55 permits H55 to rotate into the external conformation where it can hydrogen bond strongly with heme propionate 6 with distances of 2.73 and 3.21 Å in the A subunit and B subunit, respectively.

Hydrogen bonding between CO and H55 in DHPCO is likely to be even weaker than in SWMbCO. The heme moiety is located 1.5 Å deeper in DHP A than in SWMb, and the distal histidine is in the same orientation but 1.2 Å further away from heme iron than in SWMb.[32,33,79] On the basis of the comparison in Table 3, it is reasonable to estimate that the hydrogen bond energy between CO and Fe, if it exists at all, in DHP A is weaker than in SWMb. The DFT calculations carried out here corroborate this and show that the distances between the O atom of CO and the N^{ε} atom of H55 is greater than for O_2. An interaction between H55 and the heme propionate (position 6) is shown in Figure 2B and in Table 4. The short distances between the N^{δ} of H55 and the O atom of the heme propionate in DHPCO models provide an indication of the competing attraction of the heme propionates. The specific interaction with the propionate side chain appears stronger in this structure than in any corresponding structure of SWMbCO. The fact that H55 can interact in this way with the heme propionate(s) is consistent with a shift in the equilibrium toward the solvent-exposed external conformation. However, the flexibility of H55 appears to be greater than for the distal histidine in SWMbCO, which implies that the interaction with the propionate(s) is not the only factor governing the shift in equilibrium toward the solvent-exposed conformation.

Table 3. Hydrogen Bond Distances in Different Forms of Mb and DHP

crystal (PDB)	distance (Å)	crystal (PDB)	distance (Å)
Met-Mb (1a6k)	2.67	Met-DHP (2qfk)	3.14/3.24
Oxy-Mb (1mbo)	2.77	Oxy-DHP (2qfn)	2.82/2.84
CO-Mb (1dwr)	3.07	CO-DHP	3.52/>10.0

Use of DFT Calculations To Estimate the Energy of Hydrogen Bonding. DFT calculations were used to understand the effect of the internal and external conformations on the tautomeric state of H55. The DFT geometry optimizations showed that the hydrogen bond of H55 with CO is sufficiently weak that hydrogen bonding by the δ-tautomer dominates (Table 4). However, in the two O_2 structures studied, the hydrogen bonding of H55 with O_2 correlates with the ε-tautomer (PDB 2QFN). The DFT calculations are consistent with the observed CO stretching band in DHPCO at 1950 cm^{-1}, which indicates a weaker interaction with distal histidine than that observed in SWMbCO, which has a dominant band at $\nu(CO)$ = 1943 cm^{-1}.[13,14]

Relationship to Time-Resolved DHPCO X-ray Crystal Structures. The structures presented here were essential for an understanding of the time-resolved X-ray structural data.[10] The time-resolved X-ray structure provided the insight that photolyzed CO in DHP A migrates immediately to the Xe1 binding site.[82] Moreover, there is evidence for CO escape from the protein during the time course of the time-resolved X-ray experiment.[10] This trajectory is quite different from those observed in sperm whale myoglobin[83,84] and *Scapharca inequivalvis* hemoglobin[85,86] time-resolved X-ray crystal structures, where the motion of the CO is dominated by a migration to various internal Xe-binding sites after a residence in an initial docking site. There is no evidence for CO escape in either of those structures. We have noted previously in kinetic studies that CO escape is much more facile in DHP A,[13,14] which is consistent with the open conformation observed in the X-ray structures in this study.

CONCLUSION

The X-ray crystallographic structure of the DHPCO adduct provides insight into the competition between internal and external conformations of the distal histidine H55. We are compelled to modify our original model that exclusively correlates the internal and external conformations of H55 with 6- and 5-coordinate heme Fe, respectively. Contrary to this model, H55 is primarily observed in the solvent-exposed conformation in DHPCO, despite the fact that the heme Fe is 6-coordinated. The interaction of H55 with bound CO is quite weak in DHP due to the greater distance of the distal histidine from the heme Fe relative to other globins. Hydrogen bonding of the δ-tautomer of H55 with heme propionate 6 successfully competes with the Fe-bound CO. The weak interaction of H55 with bound CO is corroborated by both quantum mechanical and classical modeling to understand the energetics and dynamics, respectively. Thus, the modified model suggests that the origin of the flexibility of H55 in DHP can be found in the unique conformation of the heme, which is more deeply buried in the globin than in other myoglobins and hemoglobins. The proximity of H55 to heme propionate 6 shifts the equilibrium of the distal histidine toward the open conformation.

Table 4. Energies and Relevant Distances for the Structures Calculated by DFT Geometry Optimization

structure	energy (kcal/mol)	ΔE ($\varepsilon - \delta$) (kcal/mol)	O(CO)···Nε (Å)	O(prop)···Nδ (Å)
4GZG1_CO_H55δ	−23701	0	4.66	2.75
4GZG1_CO_H55ε	−23681	+20	3.18	6.39
2QFN1_O_2_H55δ	−23588	0	4.11	4.66
2QFN1_O_2_H55ε	−23588	0	2.88	6.08
2QFN1_CO_H55δ	−23770	0	4.53	4.99
2QFN1_CO_H55ε	−23723	−3	3.21	6.18
4GZG2_CO_H55δ	−25849	0	4.66	2.75
4GZG2_CO_H55ε	−25834	+15	3.58	5.74
2QFN2_O_2_H55δ	−25733	0	4.09	4.73
2QFN2_O_2_H55ε	−25748	−15	2.80	6.11

dx.doi.org/10.1021/bi5001905 | *Biochemistry* 2014, 53, 2474−2482

■ ASSOCIATED CONTENT

Supporting Information

Alternative views of the electron density from X-ray structures, trajectories from the molecular dynamics simulations, and coordinates of relevant structures are provided. This material is available free of charge via the Internet at http://pubs.acs.org.

■ AUTHOR INFORMATION

Corresponding Author

*E-mail: Stefan_Franzen@ncsu.edu. Phone: 919-515-8915.

Funding

The authors thank the Army Research Office for support through Grant LS-57681. We thank the National Science Foundation for funding and access to the ARC computing resource on the NCSU campus. Use of the Advanced Photon Source was supported by the U.S. Department of Energy, Basic Energy Sciences, Office of Science, under Contract No. DE-AC02-06CH11357. Use of the BioCARS Sector 14 was supported by the National Institutes of Health, National Institute of General Medical Sciences Grant P41GM103543 (formerly National Center for Research Resources P41RR007707).

Notes

The authors declare no competing financial interest.

■ ABBREVIATIONS

CO, carbon monoxide; DFT, density functional theory; DHP A, dehaloperoxidase-hemoglobin A; MD, molecular dynamics; SWMb, sperm whale myoglobin

■ REFERENCES

(1) Weber, R. E., Mangum, C., Steinman, H., Bonaventura, C., Sullivan, B., and Bonaventura, J. (1977) Hemoglobins of two terebellid polychaetes: Enoplobranchus sanguineus and Amphitrite ornata. *Comp. Biochem. Physiol. A Comp. Physiol. 56*, 179−187.

(2) Chen, Y. P., Woodin, S. A., Lincoln, D. E., and Lovell, C. R. (1996) An unusual dehalogenating peroxidase from the marine terebellid polychaete Amphitrite ornata. *J. Biol. Chem. 271*, 4609−4612.

(3) Han, K., Woodin, S. A., Lincoln, D. E., Fielman, K. T., and Ely, B. (2001) Amphitrite ornata, a marine worm, contains two dehaloperoxidase genes. *Mar. Biotechnol. 3*, 287−292.

(4) de Serrano, V., D'Antonio, J., Franzen, S., and Ghiladi, R. A. (2010) Structure of dehaloperoxidase B at 1.58 angstrom resolution and structural characterization of the AB dimer from Amphitrite ornata. *Acta Crystallogr., Sect. D: Biol. Crystallogr. 66*, 529−538.

(5) Ferrari, R. P., Laurenti, E., and Trotta, F. (1999) Oxidative 4-dechlorination of 2,4,6-trichlorophenol catalyzed by horseradish peroxidase. *JBIC, J. Biol. Inorg. Chem. 4*, 232−237.

(6) Franzen, S., Thompson, M. K., and Ghiladi, R. A. (2012) The Dehaloperoxidase Paradox. *Biochim. Biophys. Acta 1824*, 578−588.

(7) Du, J., Sono, M., and Dawson, J. H. (2010) Functional Switching of Amphitrite ornata Dehaloperoxidase from O-2-Binding Globin to Peroxidase Enzyme Facilitated by Halophenol Substrate and H_2O_2. *Biochemistry 49*, 6064−6069.

(8) D'Antonio, J., and Ghiladi, R. A. (2011) Reactivity of Deoxy- and Oxyferrous Dehaloperoxidase B from Amphitrite ornata: Identification of Compound II and Its Ferrous-Hydroperoxide Precursor. *Biochemistry 50*, 5999−6011.

(9) Lebioda, L., Dawson, J. H. X-ray Crystal Structures of Substrate-bound for of DHP, *Biochemistry*, 10.1021/bi400627w.

(10) Zhao, J., de Serrano, V., Zhao, J. J., Le, P., and Franzen, S. (2013) Structural and Kinetic Study of an Internal Substrate Binding Site in Dehaloperoxidase-Hemoglobin A from Amphitrite ornata. *Biochemistry 52*, 2427−2439.

(11) Schkolnik, G., Utesch, T., Zhao, J. J., Jiang, S., Thompson, M. K., Mroginski, M. A., Hildebrandt, P., and Franzen, S. (2013) Catalytic efficiency of dehaloperoxidase A is controlled by electrostatics - application of the vibrational Stark effect to understand enzyme kinetics. *Biochem. Biophys. Res. Commun. 430*, 1011−1015.

(12) Zhao, J. J., Rowe, J., Franzen, J., He, C., and Franzen, S. (2012) Study of the electrostatic effects of mutations on the surface of dehaloperoxidase-hemoglobin A. *Biochem. Biophys. Res. Commun. 420*, 733−737.

(13) Nienhaus, K., Deng, P., Belyea, J., Franzen, S., and Nienhaus, G. U. (2006) Spectroscopic Study of Substrate Binding to the Carbonmonoxy Form of Dehaloperoxidase from Amphitrite ornata. *J. Phys. Chem. B 110*, 13264−13276.

(14) Nienhaus, K., Nickel, E., Davis, M. F., Franzen, S., and Nienhaus, G. U. (2008) Determinants of Substrate Internalization in the Distal Pocket of Dehaloperoxidase Hemoglobin of Amphitrite ornata. *Biochemistry 47*, 12985−12994.

(15) Zhao, J., Srajer, V., and Franzen, S. (2013) Functional consequences of the open distal pocket of dehaloperoxidase-hemoglobin observed by time-resolved X-ray crystallography. *Biochemistry 52*, 7943−7950.

(16) Zhao, J. J., de Serrano, V., Dumarieh, R., Thompson, M., Ghiladi, R. A., and Franzen, S. (2012) The Role of the Distal Histidine in H_2O_2 Activation and Heme Protection in both Peroxidase and Globin Functions. *J. Phys. Chem. B 116*, 12065−12077.

(17) Nicoletti, F. P., Thompson, M. K., Howes, B. D., Franzen, S., and Smulevich, G. (2010) New insights into the role of distal histidine flexibility in ligand stabilization of Dehaloperoxidase-hemoglobin from Amphitrite ornata. *Biochemistry 49*, 1903−1912.

(18) Chen, Z., de Serrano, V., Betts, L., and Franzen, S. (2009) Distal histidine conformational flexibility in dehaloperoxidase from Amphitrite ornata. *Acta Crystallogr., Sect. D: Biol. Crystallogr. D65*, 34−40.

(19) Mukai, M., Mills, C. E., Poole, R. K., and Yeh, S. R. (2001) Flavohemoglobin, a globin with a peroxidase-like catalytic site. *J. Biol. Chem. 276*, 7272−7277.

(20) Lightning, L. K., Huang, H., Moenne-Loccoz, P., Loehr, T. M., Schuller, D. J., Poulos, T. L., and de Montellano, P. R. O. (2001) Disruption of an active site hydrogen bond converts human heme oxygenase-1 into a peroxidase. *J. Biol. Chem. 276*, 10612−10619.

(21) Sundaramoorthy, M., Terner, J., and Poulos, T. L. (1995) The crystal structure of chloroperoxidase: A heme peroxidase-cytochrome P450 functional hybrid. *Structure 3*, 1367−1377.

(22) Badyal, S. K., Joyce, M. G., Sharp, K. H., Seward, H. E., Mewies, M., Basran, J., Macdonald, I. K., Moody, P. C. E., and Raven, E. L. (2006) Conformational Mobility in the Active Site of a Heme Peroxidase. *J. Biol. Chem. 281*, 24512−24520.

(23) D'Antonio, E. L., D'Antonio, J., de Serrano, V., Gracz, H., Thompson, M. K., Ghiladi, R. A., Bowden, E. F., and Franzen, S. (2011) Functional Consequences of the Creation of an Asp-His-Fe Triad in a 3/3 Globin. *Biochemistry 50*, 9664−9680.

(24) Plummer, A., Thompson, M. K., and Franzen, S. (2013) Role of Polarity of the Distal Pocket in the Control of Inhibitor Binding in Dehaloperoxidase-Hemoglobin. *Biochemistry 52*, 2218−2227.

(25) Poulos, T. L., and Kraut, J. (1980) The stereochemistry of peroxidase catalysis. *J. Biol. Chem. 255*, 8199−8205.

(26) Vitello, L. B., Erman, J. E., Miller, M. A., Wang, J., and Kraut, J. (1993) Effect of Arginine-48 Replacement on the Reaction between Cytochrome-C Peroxidase and Hydrogen-Peroxide. *Biochemistry 32*, 9807−9818.

(27) Yang, F., and Phillips, G. N., Jr. (1996) Crystal structures of CO-, deoxy- and Met-myoglobins at various pH values. *J. Mol. Biol. 256*, 762−774.

(28) Tian, W. D., Sage, J. T., Champion, P. M., Chien, E., and Sligar, S. G. (1996) Probing Heme Protein Conformational Equilibration Rates with Kinetic Selection. *Biochemistry 35*, 3487−3502.

(29) Yuan, Y., Simplaceanu, V., Ho, N. T., and Ho, C. (2010) An Investigation of the Distal Histidyl Hydrogen Bonds in Oxyhemoglobin: Effects of Temperature, pH, and Inositol Hexaphosphate. *Biochemistry 49*, 10606−10615.

(30) Davis, M. F., Bobay, B. G., and Franzen, S. (2010) Determination of Separate Inhibitor and Substrate Binding Sites in the Dehaloperoxidase-Hemoglobin from Amphitrite ornata. *Biochemistry 49*, 1199−1206.
(31) Davis, M. F., Gracz, H., Vendeix, F. A. P., de Serrano, V., Somasundaram, A., Decatur, S. M., and Franzen, S. (2009) Different Modes of Binding of Mono-, Di-, and Trihalogenated Phenols to the Hemoglobin Dehaloperoxidase from Amphitrite ornata. *Biochemistry 48*, 2164−2172.
(32) de Serrano, V., Chen, Z., Davis, M. F., and Franzen, S. (2007) X-ray Crystal Structural Analysis of the Binding Site in the Ferric and Oxyferrous forms of the Recombinant Heme Dehaloperoxidase Cloned from Amphitrite ornata. *Acta Crystallogr., Sect. D: Biol. Crystallogr. D63*, 1094−1101.
(33) Vojtechovsky, J., Chu, K., Berendzen, J., Sweet, R. M., and Schlichting, I. (1999) Crystal structures of myoglobin-ligand complexes at near-atomic resolution. *Biophys. J. 77*, 2153−2174.
(34) Phillips, G. N., Jr., Teodoro, M. L., Li, T., Smith, B., and Olson, J. S. (1999) Bound CO Is A Molecular Probe of Electrostatic Potential in the Distal Pocket of Myoglobin. *J. Phys. Chem. B 103*, 8817−8829.
(35) Perutz, M. F., and Mathews, F. S. (1966) An X-ray Study of Azide Methaemoglobin. *J. Mol. Biol. 21*, 199−&.
(36) Royer, W. E., Jr., Pardanani, A., Gibson, Q. H., Peterson, E. S., and Friedman, J. M. (1996) Ordered water molecules as key allosteric mediators in a cooperative dimeric hemoglobin. *Proc. Natl. Acad. Sci. U. S. A. 93*, 14526−14531.
(37) Birukou, I., Soman, J., and Olson, J. S. (2011) Blocking the Gate to Ligand Entry in Human Hemoglobin. *J. Biol. Chem. 286*, 10515−10529.
(38) Cameron, A. D., Smerdon, S. J., Wilkinson, A. J., Habash, J., Helliwell, J. R., Li, T., and Olson, J. S. (1993) Distal pocket polarity in ligand binding to myoglobin: Deoxy and carbonmonoxy forms of a threonine68(E11) mutant investigated by x-ray crystallography and infrared spectroscopy. *Biochemistry 32*, 13061−13070.
(39) Ray, G. B., Li, X.-Y., Ibers, J. A., Sessler, J. L., and Spiro, T. G. (1994) How Far Can Protein Bend the FeCO Unit? Distal Polar and Steric Effects in Heme Proteins and Models. *J. Am. Chem. Soc. 116*, 162−176.
(40) Franzen, S., Roach, M. P., Chen, Y.-P., Dyer, R. B., Woodruff, W. H., and Dawson, J. H. (1998) The Unusual Reactivities of Amphitrite ornata Dehaloperoxidase and Notomastus lobatus Chloroperoxidase Do Not Arise from a Histidine Imidazolate Proximal Heme Iron Ligand. *J. Am. Chem. Soc. 120*, 4658−4661.
(41) Howes, B. D., Helbo, S., Fago, A., and Smulevich, G. (2012) Insights into the anomalous heme pocket of rainbow trout myoglobin. *J. Inorg. Biochem. 109*, 1−8.
(42) Thompson, M. K., Davis, M. F., deSorrano, V., Nicoletti, F. P., Howes, B. D., Smulevich, G., and Franzen, S. (2010) Internal Binding of Halogenated Phenols in Dehaloperoxidase-hemoglobin Inhibits Peroxidase Activity. *Biophys. J. 99*, 1586−1595.
(43) Springer, B. A., Egeberg, K. D., Sligar, S. G., Rohlfs, R. J., Mathews, A. J., and Olson, J. S. (1989) Discrimination Between Oxygen and Carbon Monoxide and Inhibition of Autooxidation by Myoglobin - Site-Directed Mutagenesis of the Distal Histidine. *J. Biol. Chem. 264*, 3057−3060.
(44) Scott, E. E., Gibson, Q. H., and Olson, J. S. (2001) Mapping the pathways for O_2 entry into and exit from myoglobin. *J. Biol. Chem. 276*, 5177−5188.
(45) Lucas, M. F., and Guallar, V. (2012) An Atomistic View on Human Hemoglobin Carbon Monoxide Migration Processes. *Biophys. J. 102*, 887−896.
(46) Capece, L., Boechi, L., Perissinotti, L. L., Arroyo-Manez, P., Bikiel, D. E., Smulevich, G., Marti, M. A., and Estrin, D. A. (2013) Small ligand-globin interactions: Reviewing lessons derived from computer simulation. *Biochim. Biophys. Acta, Proteins Proteomics 1834*, 1722−1738.
(47) Jiang, S., Wright, I., Swartz, P., and Franzen, S. (2013) The role of T56 in controlling the flexibility of the distal histidine in dehaloperoxidase-hemoglobin from Amphitrite ornata. *Biochim. Biophys. Acta, Proteins Proteomics 1834*, 2020−2029.
(48) Du, J., Huang, X., Sun, S. F., Wang, C. X., Lebioda, L., and Dawson, J. H. (2011) Amphitrite ornata Dehaloperoxidase (DHP): Investigations of Structural Factors That Influence the Mechanism of Halophenol Dehalogenation Using "Peroxidase-like" Myoglobin Mutants and "Myoglobin-like" DHP Mutants. *Biochemistry 50*, 8172−8180.
(49) Spiro, T. G., and Kozlowski, P. M. (2001) Is the CO adduct of myoglobin bent, and does it matter? *Acc. Chem. Res. 34*, 137−144.
(50) Ivanov, D., Sage, J. T., Keim, M., Powell, J. R., Asher, S. A., and Champion, P. M. (1994) Determinatino of CO Orientation in Myoglobin by Single-crystal Linear Dichroism. *J. Am. Chem. Soc. 116*, 4139−4140.
(51) Olson, J. S., and Phillips, G. N. (1997) Myoglobin discriminates between O-2, NO, and CO by electrostatic interactions with the bound ligand. *J. Biol. Inorg. Chem. 2*, 544−552.
(52) Collman, J. P., Brauman, J. I., Halbert, T. R., and Suslick, K. S. (1976) Nature of O-2 and CO Binding to Metalloporphyrins and Heme Proteins. *Proc. Natl. Acad. Sci. U.S.A. 73*, 3333−3337.
(53) Phillips, S. E. V., and Schoenborn, B. P. (1981) Neutron Diffraction Reveals Oxygen-Histidine Hydrogen Bond in Oxymyoglobin. *Nature 292*, 81−82.
(54) Slebodnick, C., and Ibers, J. A. (1997) Myoglobin models and steric origins of the discrimination between O-2 and CO. *J. Bioinorg. Chem. 2*, 521−525.
(55) Stec, B., and Phillips, G. N. (2001) How the CO in myoglobin acquired its bend: lessons in interpretation of crystallographic data. *Acta Crystallogr., Sect. D: Biol. Crystal 57*, 751−754.
(56) Franzen, S. (2002) An Electrostatic Model for the Frequency Shifts in the Carbonmonoxy Stretching Band of Myoglobin: Correlation of Hydrogen Bonding and the Stark Tuning Rate. *J. Am. Chem. Soc. 124*, 13271−13281.
(57) Vogel, K. M., Kozlowski, P. M., Zgierski, M. Z., and Spiro, T. G. (1999) Determinants of the FeXO (X = C, N, O) vibrational frequencies in heme adducts from experiment and density functional theory. *J. Am. Chem. Soc. 121*, 9915−9921.
(58) Vogel, K. M., Kozlowski, P. M., Zgierski, M. Z., and Spiro, T. G. (2000) Role of the axial ligand in heme-CO backbonding; DFT analysis of vibrational data. *Inorg. Chim. Acta 297*, 11−17.
(59) Liao, M. S., Huang, M. J., and Watts, J. D. (2013) Effects of local protein environment on the binding of diatomic molecules to heme in myoglobins. DFT and dispersion-corrected DFT studies. *J. Mol. Model. 19*, 3307−3323.
(60) Marechal, J. D., Maseras, F., Lledos, A., Mouawad, L., and Perahia, D. (2006) A DFT study on the relative affinity for oxygen of the alpha and beta subunits of hemoglobin. *J. Comput. Chem. 27*, 1446−1453.
(61) Xu, C. L., Ibrahim, M., and Spiro, T. G. (2008) DFT analysis of axial and equatorial effects on Heme-CO vibrational modes: Applications to CooA and H-NOX heme sensor proteins. *Biochemistry 47*, 2379−2387.
(62) Kozlowski, P. M., Vogel, K. M., Zgierski, M. Z., and Spiro, T. G. (2001) Steric contributions to CO binding in heme proteins: a density functional analysis of FeCO vibrations and deformability. *J. Porphyrins Phthalocyanines 5*, 312−322.
(63) De Angelis, F., Jarzecki, A. A., Car, R., and Spiro, T. G. (2005) Quantum chemical evaluation of protein control over heme ligation: CO/O-2 discrimination in myoglobin. *J. Phys. Chem. B 109*, 3065−3070.
(64) Marti, M. A., Crespo, A., Capece, L., Boechi, L., Bikiel, D. E., Scherlis, D. A., and Estrin, D. A. (2006) Dioxygen affinity in heme proteins investigated by computer simulation. *J. Inorg. Biochem. 100*, 761−770.
(65) Otwinowski, Z., and Minor, W. (1997) Processing of x-ray diffraction data collected in oscillation mode. *Methods Enzymol. 276*, 307−326.
(66) Krissinel, E. B., Winn, M. D., Ballard, C. C., Ashton, A. W., Patel, P., Potterton, E. A., McNicholas, S. J., Cowtan, K. D., and Emsley, P.

(2004) The new CCP4 Coordinate Library as a toolkit for the design of coordinate-related applications in protein crystallography. *Acta Crystallogr., Sect. D: Biol. Crystallogr. D60*, 2250−2255.
(67) Potterton, L., McNicholas, S., Krissinel, E., Gruber, J., Cowtan, K., Emsley, P., Murshudov, G. N., Cohen, S., Perrakis, A., and Noble, M. (2004) Developments in the CCP4 molecular-graphics project. *Acta Crystallogr., Sect. D: Biol. Crystallogr. D60*, 2288−2294.
(68) Emsley, P., and Cowtan, K. (2004) Coot: model-building tools for molecular graphics. *Acta Crystallogr., Sect. D: Biol. Crystallogr. D60*, 2126−2132.
(69) Delley, B. (1990) An all-electron numerical method for solving the local density functional for polyatomic molecules. *J. Chem. Phys. 92*, 508−517.
(70) Delley, B. (2000) From molecules to solids with the DMol3 approach. *J. Chem. Phys. 113*, 7756−7764.
(71) Perdew, J. P., Burke, K., and Wang, Y. (1996) Generalized gradient approximation for the exchange-correlation hole of a many-electron system. *Phys. Rev. B: Condens. Matter 54*, 16533−16539.
(72) Mermin, N. D. (1965) Thermal properties of a homogeneous electron gas. *Phys. Rev. A 137*, 1441−1443.
(73) Humphrey, W., Dalke, A., and Schulten, K. (1996) VMD: Visual molecular dynamics. *J. Mol. Graph. 14*, 33−38.
(74) Nelson, M. T., Humphrey, W., Gursoy, A., Dalke, A., Kale, L. V., Skeel, R. D., and Schulten, K. (1996) NAMD: A parallel, object oriented molecular dynamics program. *Int. J. Supercomput. Appl. High Perform. Comput. 10*, 251−268.
(75) Phillips, J. C., Braun, R., Wang, W., Gumbart, J., Tajkhorshid, E., Villa, E., Chipot, C., Skeel, R. D., Kale, L., and Schulten, K. (2005) Scalable molecular dynamics with NAMD. *J. Comput. Chem. 26*, 1781−1802.
(76) Kuriyan, J., Wilz, S., Karplus, M., and Petsko, G. A. (1986) X-ray Structure and Refinement of Carbon Monoxy (Fe-II)-Myoglobin at 1.5 Å Resolution. *J. Mol. Biol. 192*, 133−154.
(77) de Serrano, V. S., Davis, M. F., Gaff, J. F., Zhang, Q., Chen, Z., D'Antonio, E. L., Bowden, E. F., Rose, R., and Franzen, S. (2010) X-ray structure of the metcyano form of dehaloperoxidase from Amphitrite ornata: evidence for photoreductive dissociation of the iron-cyanide bond. *Acta Crystallogr., Sect. D: Biol. Cryst. 66*, 770−782.
(78) Smirnova, T. I., Weber, R. T., Davis, M. F., and Franzen, S. (2008) Substrate Binding Triggers a Switch in the Iron Coordination in Dehaloperoxidase from Amphitrite ornata: HYSCORE Experiments. *J. Am. Chem. Soc. 130*, 2128−2129.
(79) LaCount, M. W., Zhang, E., Chen, Y. P., Han, K., Whitton, M. M., Lincoln, D. E., Woodin, S. A., and Lebioda, L. (2000) The crystal structure and amino acid sequence of dehaloperoxidase from Amphitrite ornata indicate common ancestry with globins. *J. Biol. Chem. 275*, 18712−18716.
(80) Hanson, J. C., and Schoenborn, B. P. (1981) Real Space Refinement of Neutron Diffraction Data from Sperm Whale Carbonmonoxy Myoglobin. *J. Mol. Biol. 153*, 117−146.
(81) Sigfridsson, E., and Ryde, U. (1999) On the significance of hydrogen bonds for the discrimination between CO and O_2 by myoglobin. *J. Biol. Inorg. Chem. 4*, 99−110.
(82) De Serrano, V., and Franzen, S. (2012) Structural Evidence for Stabilization of Inhibitor Binding by a Protein Cavity in the Dehaloperoxidase-Hemoglobin from Amphitrite ornata. *Peptide Sci. 98*, 27−35.
(83) Cho, H. S., Dashdorj, N., Schotte, F., Graber, T., Henning, R., and Anfinrud, P. (2010) Protein structural dynamics in solution unveiled via 100-ps time-resolved x-ray scattering. *Proc. Natl. Acad. Sci. U.S.A. 107*, 7281−7286.
(84) Schotte, F., Lim, M. H., Jackson, T. A., Smirnov, A. V., Soman, J., Olson, J. S., Phillips, G. N., Wulff, M., and Anfinrud, P. A. (2003) Watching a protein as it functions with 150-ps time-resolved X-ray crystallography. *Science 300*, 1944−1947.
(85) Knapp, J. E., Pahl, R., Cohen, J., Nichols, J. C., Schulten, K., Gibson, Q. H., Srajer, V., and Royer, W. E. (2009) Ligand Migration and Cavities within Scapharca Dimeric Hbl: Studies by Time-Resolved Crystallography, Xe Binding, and Computational Analysis. *Structure 17*, 1494−1504.
(86) Knapp, J. E., Pahl, R., Srajer, V., and Royer, W. E. (2006) Allosteric action in real time: Time-resolved crystallographic studies of a cooperative dimeric hemoglobin. *Proc. Natl. Acad. Sci. U. S. A. 103*, 7649−7654.